

Chapter 4

Identifying Damage Location

4.1 Time Domain Approach

In the conventional impedance-based structural health monitoring technique using only the electrical self admittance, its limited sensing area makes it relatively easy to tell where the damage is present: the damage exists near the PZT which detects it. However, this technique requires a large number of PZTs to monitor a large area. On the other hand, as demonstrated in Chapter 3, using the electrical transfer admittance could extend the sensing area of the impedance-based technique and could reduce the number of PZT sensor-actuators. Damage located far from the PZT can also be detected. However, this may make it difficult to identify the location of damage because the damage is not necessarily near the PZT sensor-actuator.

In order to assess the damage location, a time domain approach using multiple piezoelectric sensors and actuators is investigated in this chapter. The basic idea is from the pulse-echo method which is often used in ultrasonic inspection. Figure 4.1 shows the principle of the pulse-echo method [34]. When an ultrasonic pulse travels through a test piece and strikes a crack or some other damage, it will be reflected. It will show up as an echo pulse in the time history chart. Since the wave speed in a material is normally constant, the time-base of the chart is directly correlated to the distance traveled. The wave speed can be calculated from the length of the test piece and the time difference between the initial echo and the back echo. Thus, we can assess the damage location by tracking the flaw echo.

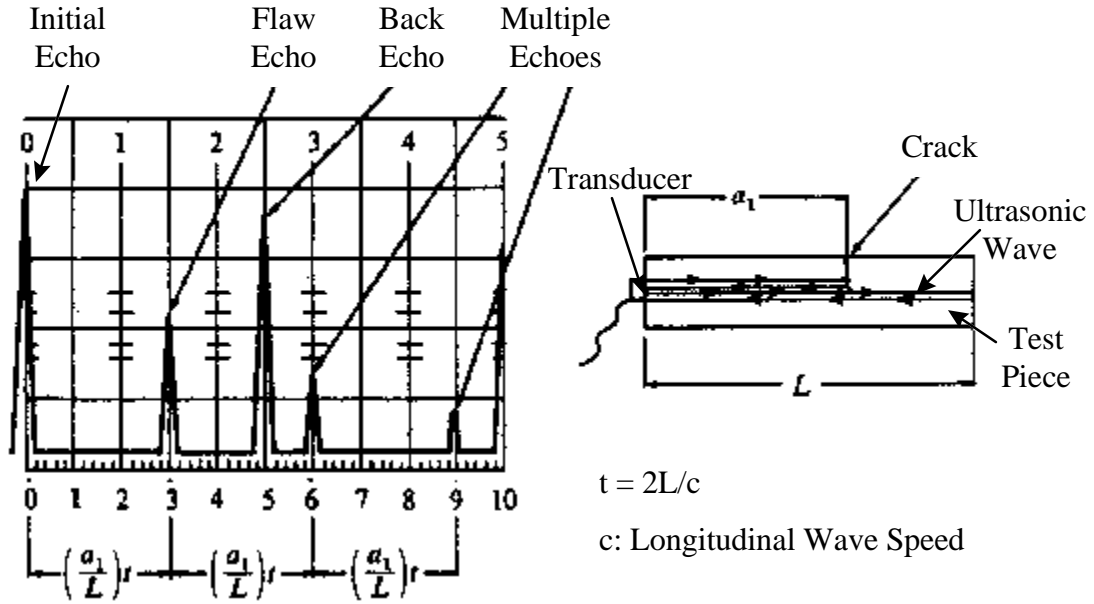


Figure 4.1: Principle of the pulse-echo method in ultrasonic inspection [34]

However, the manner of reflections will be complicated if the wave propagation cannot be considered one-dimensional (1-D). It is not practical to apply this method to 2-D or 3-D cases. Therefore, only 1-D model such as a uniform rod is dealt here.

The 1-D wave equation [35] can be expressed as:

$$\frac{\partial^2 u(x,t)}{\partial t^2} = c_l^2 \frac{\partial^2 u(x,t)}{\partial x^2} \quad (4.1)$$

$$c_l = \sqrt{\frac{\lambda + 2\mu}{\rho}} \quad (4.2)$$

$$\lambda = \frac{\nu E}{(1+\nu)(1-2\nu)}, \quad \mu = \frac{E}{2(1+\nu)} \quad (4.3)$$

where $u(x,t)$ is the displacement at position x and time t , c_l is the pure longitudinal wave speed, λ and μ are the Lamé constants, ρ is the mass density, E is the Young's modulus, and

ν is the Poisson's ratio.

In this case, it is assumed that there is no lateral strain because all material elements move purely in the direction of propagation. However, the presence of longitudinal stress will produce associated lateral strains through the Poisson contraction phenomenon in bars or beams because they have one or more outer surfaces free from constraints. Hence, pure longitudinal wave motion cannot occur and the term “quasi-longitudinal” is used. The quasi-longitudinal wave equation [36] is:

$$\frac{\partial^2 u(x,t)}{\partial t^2} = c^2 \frac{\partial^2 u(x,t)}{\partial x^2} \quad (4.4)$$

$$c = \sqrt{\frac{E}{\rho}} \quad (4.5)$$

where c is the quasi-longitudinal wave speed.

The quasi-longitudinal wave speed calculated by Equation (4.5) can be used to check the validity of the wave speed obtained by the experiment.

4.2 Excitation Technique

Instead of ultrasonic transducers, multiple piezoelectric sensors and actuators are used for the feasibility study on identifying damage location since they are assumed to already be bonded on the structure for the impedance-based structural health monitoring. The piezoelectric sensor-actuator here is basically a thin PZT patch. In this case, we have to be careful about the wave form generated by the PZT. That is, the transverse or bending wave is rather dominant, while the longitudinal wave is required for the pulse-echo method. Figure 4.2 shows the deformation patterns of various types of waves. In this section, an excitation technique to

generate longitudinal wave is investigated experimentally.

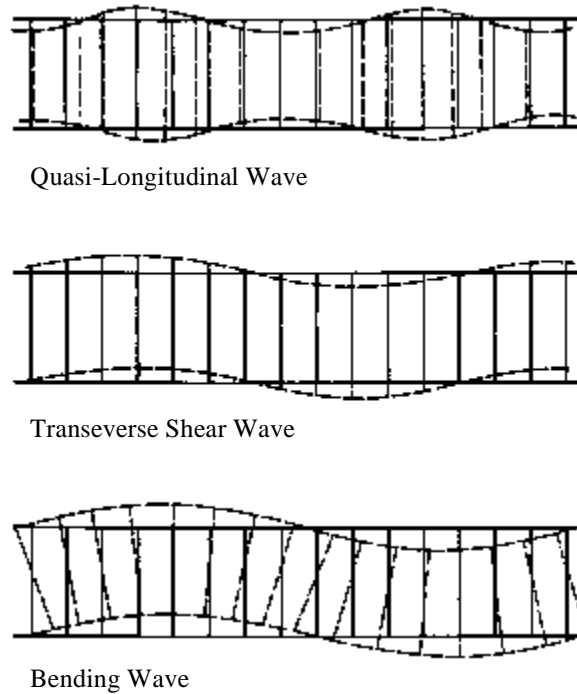


Figure 4.2: Deformation patterns of various types of waves [36]

Figure 4.3 shows a schematic of the experiment. Three PZTs (Piezo Systems PSI-5A, 30 mm x 30 mm x 0.254 mm) were bonded on a free-free brass beam (1220 mm x 38.5 mm x 4.85 mm). PZT 1 was bonded on one side of the beam, PZT 2 was on the other side of the beam from PZT 1, and PZT 3 was on the other end of the beam. A Hewlett-Packard function generator (model HP3314A) applied an excitation pulse (2.5 V) to PZT 1 and/or PZT 2 and the traveling pulse was captured by PZT 3. The excitation pulse was used for the measurement trigger and the time domain signals of the excitation input and the response at PZT 3 were sampled every 9.765625 μ s simultaneously. A ZONIC analyzer (WCA model) was used for data acquisition. Three sets of measurement were taken: i) PZT 1 excitation only; ii) PZT 2 excitation only; and iii) both PZT 1 and 2 excited in phase.

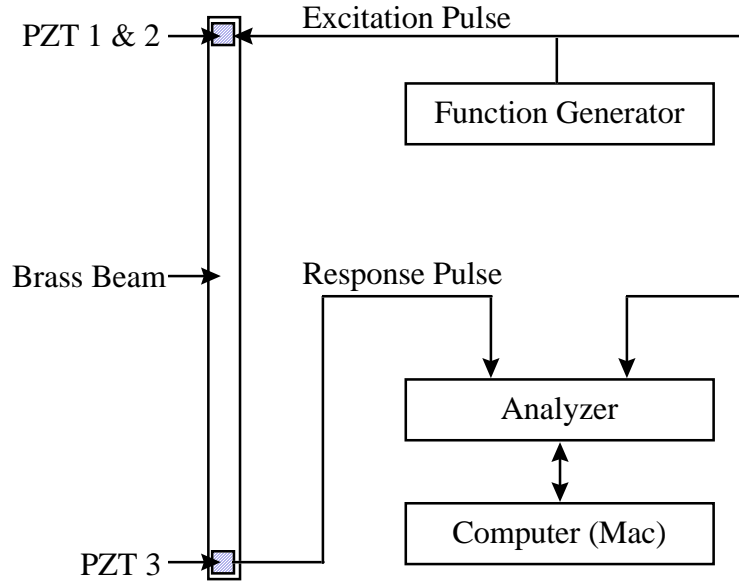


Figure 4.3: Schematic of the beam excitation test

Figure 4.4 demonstrates the experimental results and each plot shows the response at PZT 3. The initial pulse was applied to PZT 1 and/or PZT 2 at 0 on the time axis. The first plot is the result of PZT 1 excitation only. We can find the traveling pulse at about 0.4 ms. However, no back echo can be recognized after this because the bending vibration is dominant. The second one is the result of PZT 2 excitation only. The same thing as the first one can be said for this plot, while the bending direction is opposite. The third one is the result of the simultaneous in phase excitation of PZT 1 and 2. In this case, back echoes can be clearly found and they appear every 0.6348 ms. Since the length of the beam is 1220 mm, the wave speed can be calculated as follows:

$$c = \frac{2L}{t} = \frac{2 \times 1220 \times 10^{-3}}{0.6348 \times 10^{-3}} = 3844 \text{ [m / s]}$$

On the other hand, the wave speed calculated by Equation (4.5) is:

$$c = \sqrt{\frac{E}{\rho}} = \sqrt{\frac{10.0 \times 10^{10}}{8.5 \times 10^3}} = 3430 \text{ [m / s]}$$

Because they are close, the wave may be considered as longitudinal. Thus, it is confirmed that the simultaneous in phase excitation of two PZTs can produce a longitudinal wave.

The last plot is the summation of PZT 1 excitation and PZT 2 excitation. Though it is not as good as the simultaneous excitation, most of the back echoes can be recognized. This implies that the superposition may be available, *i.e.*, a longitudinal wave response may be constructed by a simple linear calculation without the simultaneous excitation. It will be very useful when the structure is complicated or simultaneous excitation is not available.

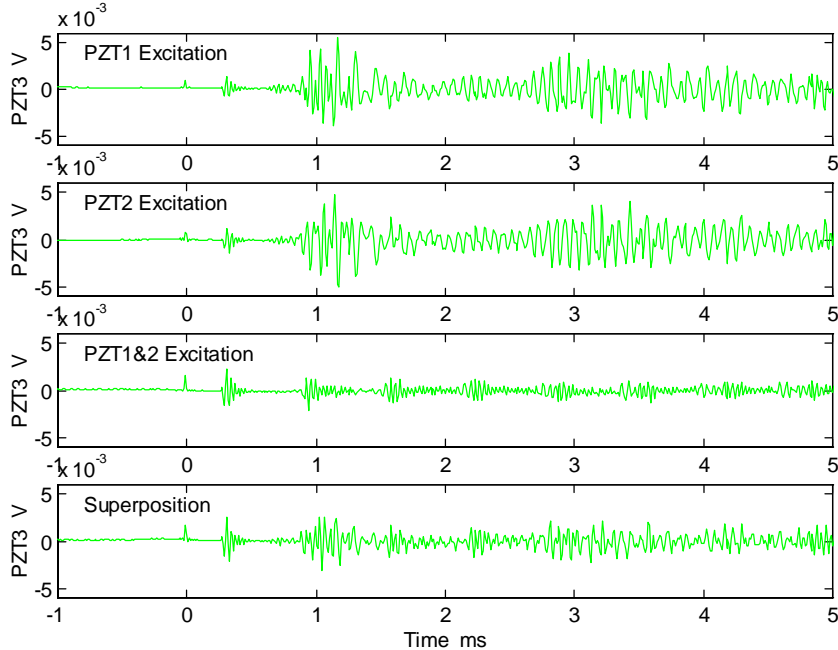


Figure 4.4: Experimental results by various types of excitation

4.3 Wavelet Analysis

In the previous sections, it was presented that we could identify the damage location by tracking a longitudinal wave propagating through a structure in time domain and the longitudinal wave could be generated by the simultaneous in phase excitation of two PZTs or the superposition calculation. However, finding and tracking the traveling pulse in the measured

data is sometimes difficult since the data may be contaminated by noise. In this section, a methodology based on wavelet decomposition to extract the traveling pulse from the noisy data is demonstrated.

There are many signal analysis tools and perhaps the most well-known of those is Fourier analysis which is expressed as:

$$F(\omega) = \int_{-\infty}^{\infty} f(t)e^{-j\omega t} dt \quad (4.6)$$

where $F(\omega)$ is Fourier transform of $f(t)$, ω is the angular frequency, $f(t)$ is the function of time, and t is the time.

For many signals, Fourier analysis is extremely useful because the frequency content of the signal is very important. Nevertheless, Fourier analysis has a serious drawback. In transforming to the frequency domain, time information is lost. When looking at a Fourier transform of a signal, it is impossible to tell when a particular event took place.

The Short-Time Fourier Transform (STFT), which analyzes only a small section of the signal at a time, corrects this deficiency. Its mathematical expression is shown below.

$$F(\omega, \tau) = \int_{-\infty}^{\infty} f(t)w(t - \tau)e^{-j\omega t} dt \quad (4.7)$$

where $w(t)$ is the window function, and τ is the position in time.

The STFT maps a signal into a two-dimensional function of time and frequency. It provides some information about both when and at what frequencies a signal event occurs. However, the STFT also has a drawback. That is, the precision of the time-frequency information is limited by the size of the window. Once we choose a particular size of the

window function, the window is the same for all frequencies. Many signals require a more flexible approach. In most cases, we need a high frequency resolution at low frequencies and a high time resolution at high frequencies.

Wavelet analysis [37], [38], [39], which has a variable-sized window, is a solution of this problem. The wavelet transform is defined as:

$$W(a, \tau) = \frac{1}{\sqrt{a}} \int_{-\infty}^{\infty} f(t) \psi\left(\frac{t-\tau}{a}\right) dt \quad (4.8)$$

where $W(a, \tau)$ is the wavelet transform or wavelet coefficients, a is the scale, and ψ is the wavelet function or mother wavelet.

Wavelet analysis allows the use of long time intervals where we want more precise low frequency information, and shorter regions where we want high frequency information. The scale factor, a , is to stretch or compress the wavelet function and is inversely related to the frequency, ω . Figure 4.5 shows the difference between the STFT and the wavelet transform.

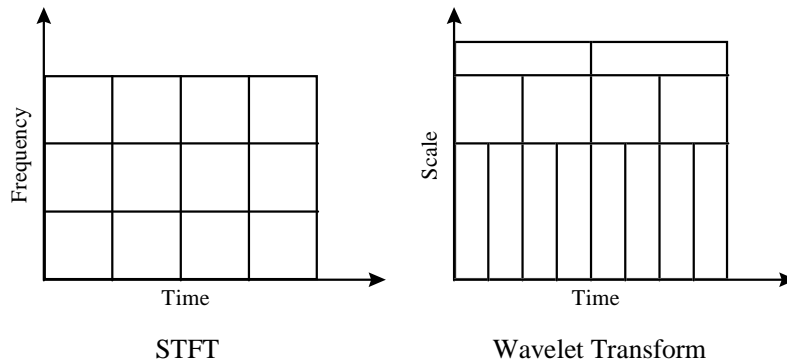


Figure 4.5: Comparison of STFT and wavelet transform

One major advantage afforded by wavelet analysis is the ability to perform local analysis, *i.e.*, to analyze a localized area of a large signal. For example, a small discontinuity,

perhaps too tiny to be seen in a plot of a continuous signal, can be found by using wavelet analysis.

Thus, in order to extract traveling pulses from a noisy signal, wavelet analysis can be applied. A simple numerical simulation was performed to validate this approach. Figure 4.6 shows a schematic of the simulation model and Figure 4.7 shows the input and the output signal.

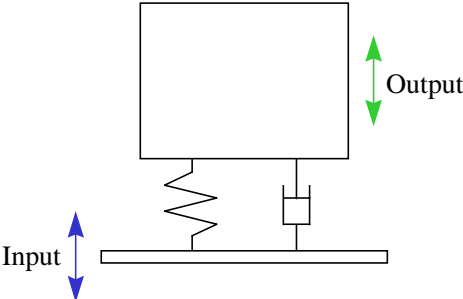


Figure 4.6: Schematic of the simulation model

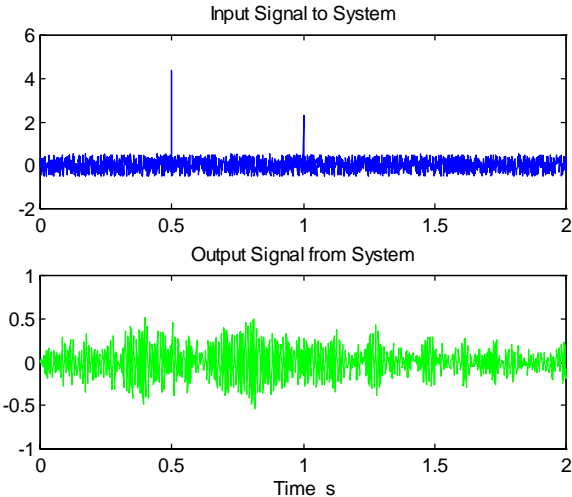


Figure 4.7: Input and output signal of the simulation

The model consists of a mass, a damper and a spring, *i.e.*, a single degree of freedom (SDOF) system. The natural frequency, the damping ratio and the sampling frequency are

assumed to be 100 Hz, 0.03 and 1 kHz, respectively. The input signal to the system consists of two pulses together with white noise. The pulses appear at 0.5 s and 1.0 s as can be seen in the plot. However, the pulses in the output signal are almost invisible. Detecting this kind of signal is needed in real structural health monitoring.

The discrete wavelet decomposition was used to extract the pulses from the output signal. The decomposition was performed by using the MATLAB Wavelet Toolbox [40]. Figure 4.8 demonstrates the result of the wavelet decomposition. In this case, Daubechies wavelet 'db8' was used. The output signal, s , was decomposed into the approximation, $a1$, and the detail, $d1$. The approximation is the high-scale, low-frequency component of the signal and the detail is the low-scale, high-frequency component.

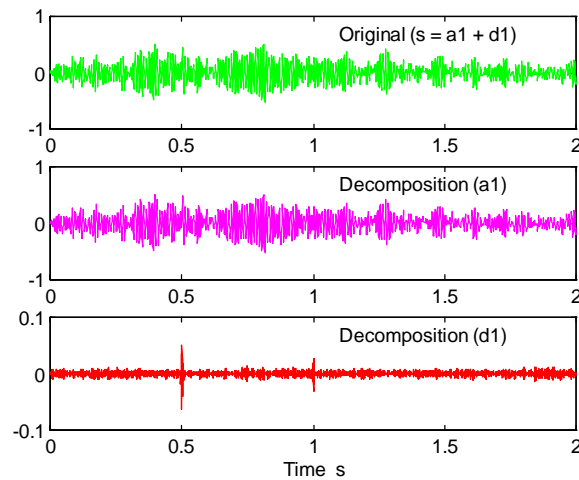


Figure 4.8: Wavelet decomposition of the output signal

We can clearly recognize the pulses at 0.5 s and 1.0 s in the plot of $d1$, while they are invisible in the original signal. This result indicates that the discrete wavelet decomposition is very useful to extract traveling pulses from a noisy signal, which must be detected to identify damage location.

4.4 Experimental Results

A proof of concept experiment on a free-free aluminum beam was carried out. Figure 4.9 shows a schematic of the experiment.

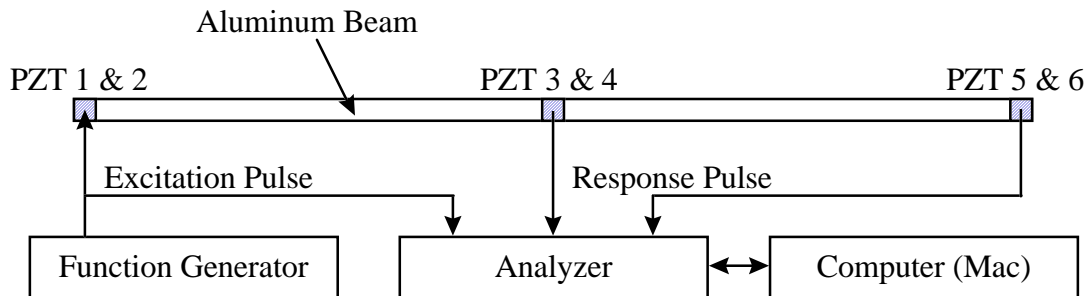


Figure 4.9: Schematic of the experiment on damage location

Six PZTs (Piezo Systems PSI-5A, 12.7 mm x 12.7 mm x 0.254 mm) were bonded on a free-free aluminum beam (1830 mm x 12.7 mm x 3.18 mm). PZT 1 was bonded on an edge of the beam, PZT 2 was on the other side of PZT 1, PZT 3 was on the middle of the beam, PZT 4 was on the other side of PZT 3, PZT 5 was on the other edge and PZT 6 was on the other side of PZT 5. A Hewlett-Packard function generator (model HP3314A) applied an excitation pulse (2.5 V) to a pair of PZTs, such as PZT 1&2, PZT 3&4 or PZT 5&6, to produce a longitudinal wave. The excitation pulse was used for measurement trigger and the time domain signals of the excitation input and the responses were sampled every 9.765625 μ s simultaneously. A ZONIC analyzer (WCA model) was used for data acquisition. Damage was simulated by putting a small aluminum clamp (26 mm x 10 mm x 1 mm) on the beam.

The location of damage on the beam, whose dimension is shown in Figure 4.10, can be assessed by the following steps. At first, PZT 1 and 2 are used as actuators to generate a pulse and PZT 3 is used as a sensor.

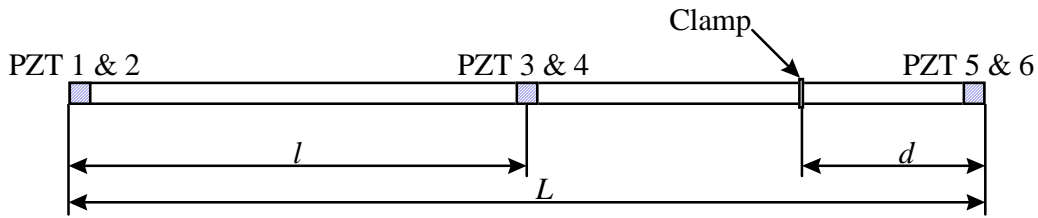


Figure 4.10: Dimension of the beam

Step 1: Calculate the wave speed (Figure 4.11)

The wave speed, c , can be calculated from the measurement in the healthy case as follows:

$$c = \frac{l}{t_1} \quad (4.9)$$

where c is the wave speed, l is the distance between PZT 1&2 and PZT 3&4, and t_1 is the time when the first echo arrives at PZT 3.

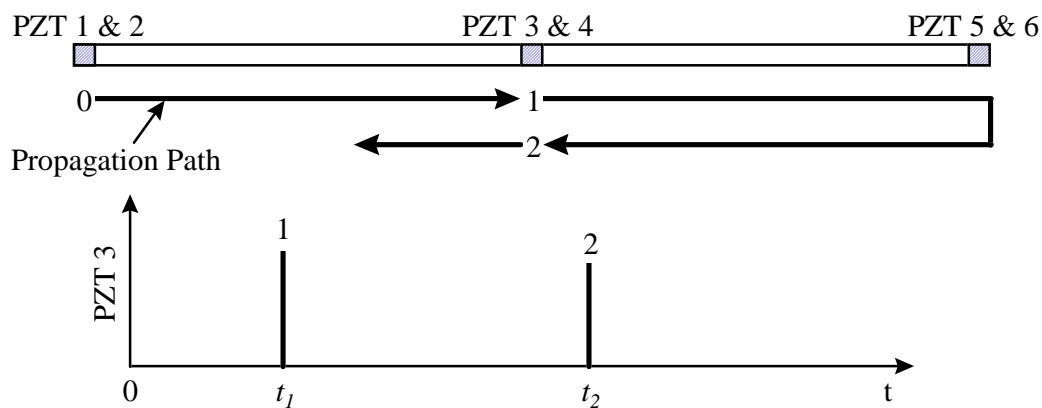


Figure 4.11: Wave propagation in healthy (without clamp) case with PZT 1&2 excitation

Step 2: Find a new pulse caused by damage and calculate the damage location (Figure 4.12)

A new pulse between the pulse 1 and 2 will be found in the damaged (with clamp) case.

The damage location can be calculated as follows:

$$d = L - l - \frac{c(t_A - t_1)}{2} \quad (4.10)$$

where d is the location of the damage (distance from the edge, Figure 4.10), L is the length of the beam, and t_A is the time when the reflection echo caused by the damage arrives at PZT 3.

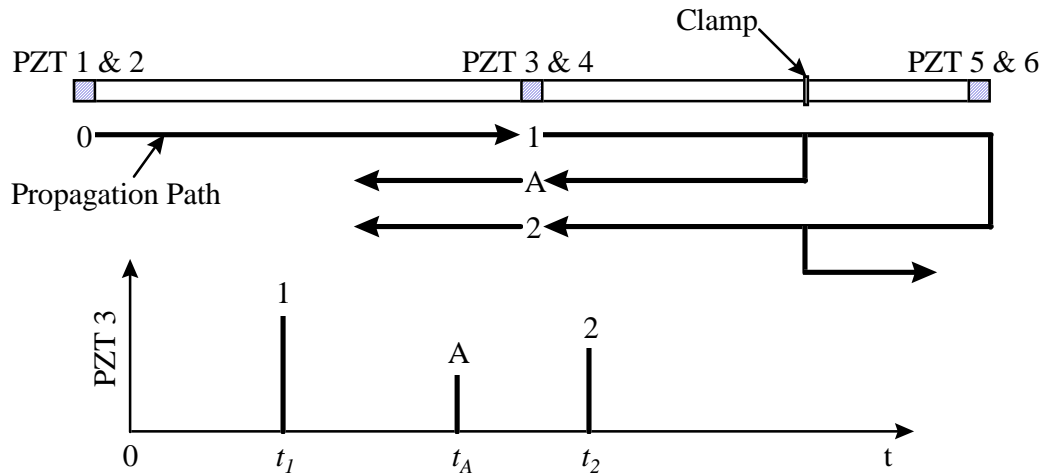


Figure 4.12: Wave propagation in damaged (with clamp) case with PZT 1&2 excitation

If the damage is present wherever on the beam, the new pulse A must appear between the pulse 1 and 2. However, there is another possible damage location for the pulse pattern in Figure 4.12, *i.e.*, the damage may be present between PZT 1&2 and PZT 3&4 instead of between PZT 3&4 and PZT 5&6. Figure 4.13 shows another possible case.

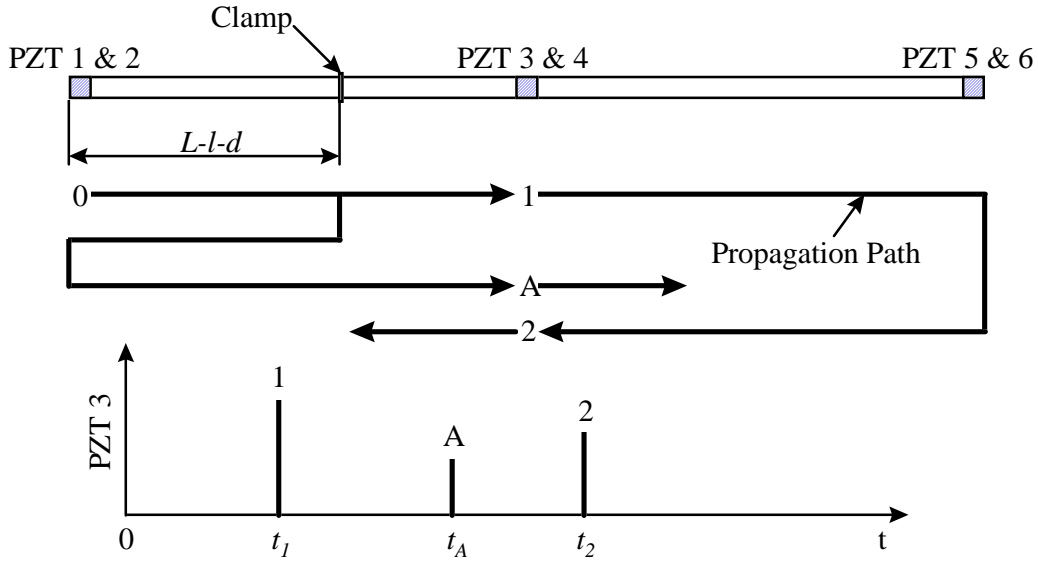


Figure 4.13: Wave propagation in another damaged (with clamp) case

Therefore, another measurement is required to obtain a unique solution, *i.e.*, to identify the damage location.

Step 3: Take another measurement (Figure 4.14)

The measurement here is taken by using PZT 5&6 as actuators and PZT 3 as a sensor. The damage location can be calculated as follows:

$$d' = \frac{c(t_A' - t_1')}{2} \quad (4.11)$$

where d' is the location of the damage (distance from the edge), t_A' is the time when the reflection echo caused by the damage arrives at PZT 3, and t_1' is the time when the first echo arrives at PZT 3.

Step 4: Compare two measurements

If d equals d' , then the damage location should be d from the edge of PZT 5&6 side

as shown in Figure 4.10. If d is not equal to d' , the damage should be present $L-l-d$ from the edge of PZT 1&2 side as shown in Figure 4.13. Thus, the damage location can be identified.

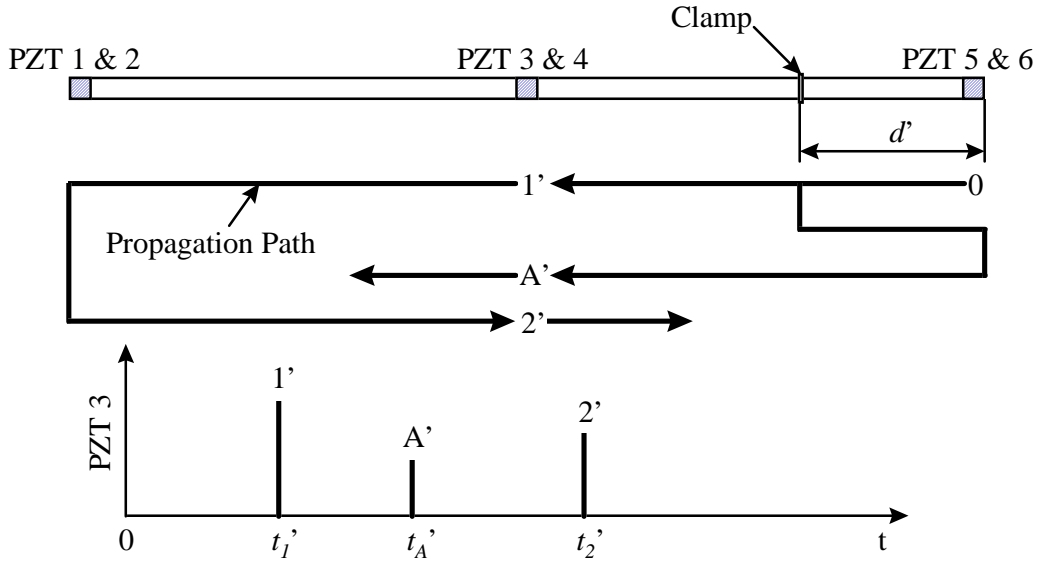


Figure 4.14: Wave propagation in damaged (with clamp) case with PZT 5&6 excitation

In the experiment, the parameters of the beam were as follows: $L = 1830$ mm, $l = 915$ mm and $d = 400$ mm. Figure 4.15 shows the result of PZT 1&2 excitation. All the plots are the time domain data captured by PZT 3. The plots on the left hand side demonstrate the original signals and those on the right hand side are the results of wavelet decomposition. In fact, the original signals in this case are not so noisy and we can track the traveling pulse. However, the wavelet decomposition makes the pulses clearer. Hence, the results of wavelet decomposition are used to determine t_1 and t_A .

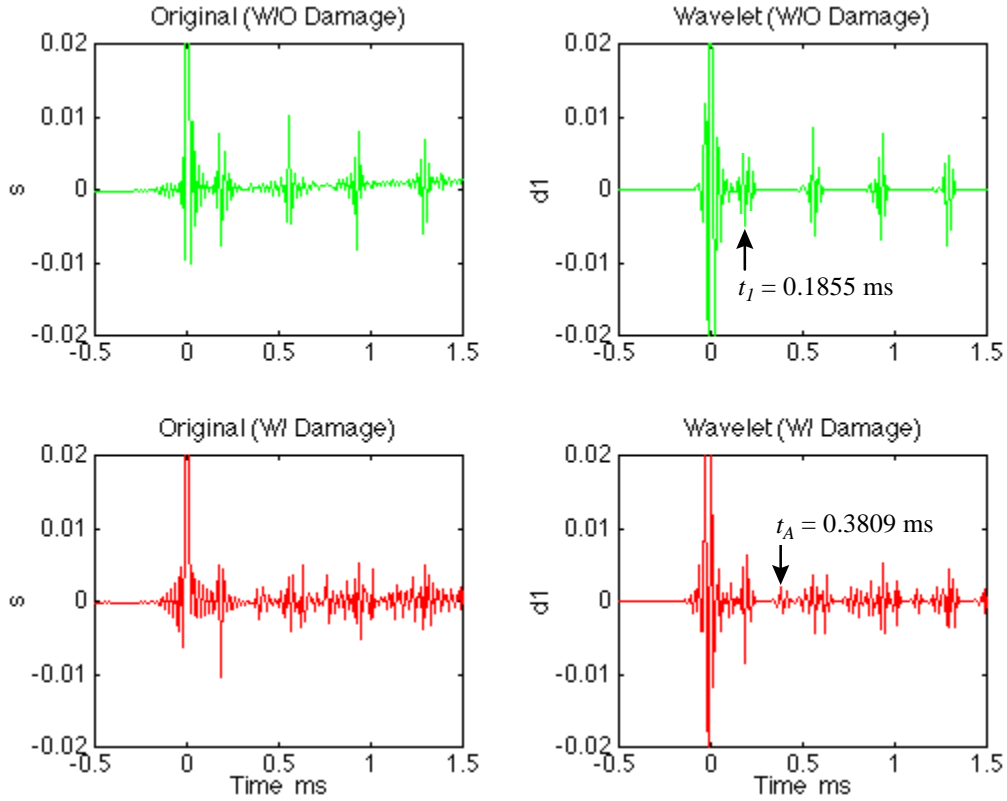


Figure 4.15: Damage location experiment (Excitation: PZT 1&2, Measurement: PZT 3)

At first, the wave speed can be obtained by Equation (4.9).

$$c = \frac{l}{t_1} = \frac{915}{0.1855} = 4933 \text{ [m / s]}$$

On the other hand, Equation (4.5) gives the following result.

$$c = \sqrt{\frac{E}{\rho}} = \sqrt{\frac{7.0 \times 10^{10}}{2.7 \times 10^3}} = 5092 \text{ [m / s]}$$

Therefore, we can say that the wave speed calculated by Equation (4.9) is reasonable.

Next, the damage location can be obtained by Equation (4.10).

$$d = L - l - \frac{c(t_A - t_1)}{2} = 1830 - 915 - \frac{4933 \times (0.3809 - 0.1855)}{2} = 433 \text{ [mm]}$$

Let's think about the spatial resolution here. The wave speed is 4933 m/s and the sampling period of the analyzer is 9.765625 μ s. Then, the resolution, Δd , is:

$$\Delta d = 4933 \times 10^3 \times 9.765625 \times 10^{-6} = 48 \text{ [mm]}$$

Recall that the true damage location is at 400 mm. Since the true value is between $d - \Delta d$ and $d + \Delta d$, it can be said that the estimated damage location is quite accurate.

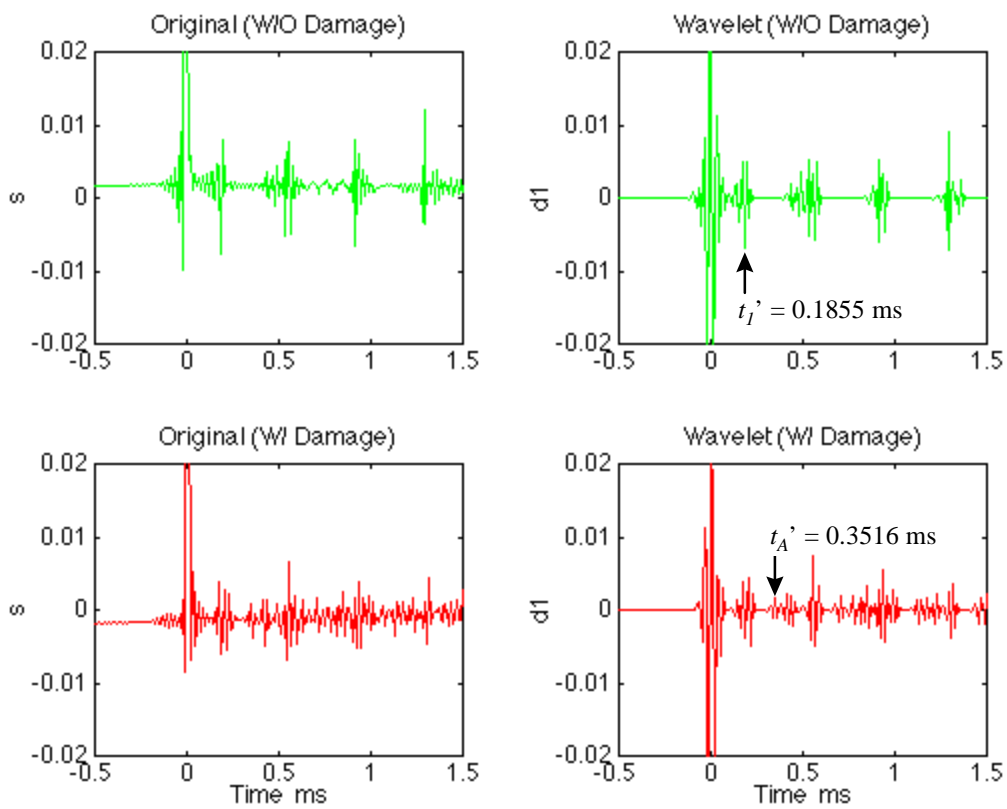


Figure 4.16: Damage location experiment (Excitation: PZT 5&6, Measurement: PZT 3)

Figure 4.16 shows the result of PZT 5&6 excitation. All the plots are the time domain data captured by PZT 3 as well as Figure 4.15. The wave speed from this result is also 4933 m/s because $t_1' = t_1 = 0.1855$ ms. The damage location can be calculated by Equation (4.11).

$$d' = \frac{c(t_A' - t_1')}{2} = \frac{4933 \times (0.3516 - 0.1855)}{2} = 410 \text{ [mm]}$$

From the results of two experiments, the location of damage can be assessed as 421.5 mm (average of $d = 433$ mm and $d' = 410$ mm), while the true value is 400 mm. The estimation can be considered good. The error is caused by the resolution which depends on the sampling period. If more accurate damage locations are required, shorter sampling periods are required.

Incidentally, the pulse at 0 ms, where no signal should be present, is due to the input signal. Since the aluminum beam is electrically conductive and the beam is used as common ground, PZT 3 receives the input pulse. However, there is no direct influence of the input on the measurement after this moment.

4.5 Conclusions

A damage location technique based on the time domain pulse-echo method was developed. This technique utilizes multiple piezoelectric sensors and actuators, which can also be used for the impedance-based structural health monitoring. Its validity was demonstrated through the proof of concept experiment on a free-free aluminum beam. The location of damage, which was simulated by a tiny clamp, on the beam was successfully identified. Thus, if we combine this damage location technique with the new impedance-based structural health monitoring technique which uses the electrical transfer admittance to extend the sensing area, we will be able to detect a distant damage and will also be able to assess the location of the damage.

The presented damage location technique contains two useful techniques. The first one is to generate a longitudinal wave which is needed for damage location. It was shown experimentally that simultaneous in phase excitation of a pair of PZTs could generate a

longitudinal wave. Moreover, when the structure in question is complicated or simultaneous excitation is not available, simple superposition calculation may construct a longitudinal wave propagation numerically.

The second one is to extract a traveling pulse from a noisy signal. Sometimes, telling when the pulse arrives at the sensor location in the captured time domain data is difficult due to noise or undesired wave motion, however, the precise information of the arriving time is necessary to identify the damage location accurately. A simulation indicated that the wavelet decomposition was very useful for solving this problem. Even “invisible” pulses were successfully extracted by this approach.

The spatial resolution in the demonstration was not so fine since the data sampling (about 100kHz) was not fast enough. A higher sampling frequency is necessary for better resolution. The high frequency sampling is good not only for improving the resolution but also for extracting the traveling pulse. When the sampling frequency is high, we can use a narrow width pulse as an initial excitation. The narrow width pulse has a very high frequency component, while the frequencies of noise such as bending modes are relatively low. The difference in frequency components will make the extraction easier.